This is an open access article published under an ACS AuthorChoice License, which permits copying and redistribution of the article or any adaptations for non-commercial purposes.

ACS OMEGA

Article

Cite This: ACS Omega 2019, 4, 5412−5423

http://pubs.acs.org/journal/acsodf

Rheological and Mechanical Investigation into the Effect of Different Molecular Weight Poly(ethylene glycol)s on Polycaprolactone-Ciprofloxacin Filaments

Mohammed Elbadawi*

Control Engineering Group, Department of Computer Science, Electrical and Space Engineering, Luleå University of Technology, SE-97187 Luleå, Sweden

Supporting Information

ABSTRACT: Fused deposition fabrication (FDF) three-dimensional printing is a potentially transformative technology for fabricating pharmaceuticals. The state-of-the-art technology is still in its infancy and requires a concerted effort to realize its potential. One aspect includes the processing parameters of FDF and the effect of formulation thereto, which, to date, have not been thoroughly investigated. To progress understanding, the effect of different molecular weight poly(ethylene glycol)s (PEG) on polycaprolactone (PCL) loaded with ciprofloxacin (CIP) was investigated. A rheometer was used, and adapted accordingly, to analyze three processing aspects pertaining to FDF: viscosity, solidification, and adhesion. The results revealed that both CIP and PEG affected all three processing parameters. The salient findings were that the ternary blend with 10% w/w PEG 8000 exhibited rheological and adhesive properties ideal for FDF, as it provided a desirably shear-thinning filament that solidified rapidly, and improved the adhesion strength, in comparison to both the PCL-CIP binary blend and other ternary blends. In contrast, the ternary blend with 15% w/w PEG 200 was unfavorable; despite having a greater plasticizing effect, whereby the viscosity was markedly reduced, the sample provided no benefit to the solidification behavior of PCL-CIP and, in addition, failed to display adhesive behavior, which is a necessity for a successful print in FDF. The original findings herein set the precedent that the effect of drug and PEG on FDF processing should be considered beyond solely modifying the viscosity.

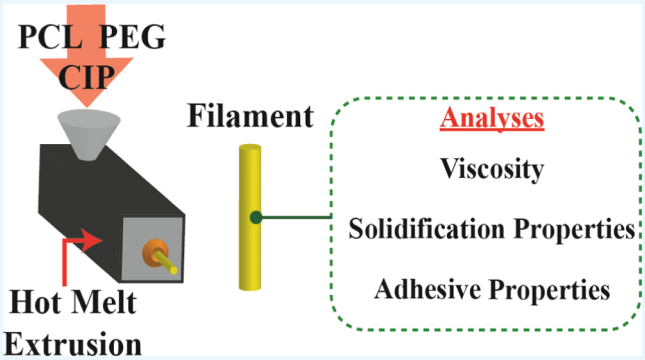

1. INTRODUCTION

Fused deposition fabrication (FDF) is a form of additive manufacturing (AM), and has recently garnered attention for fabricating drug-delivery systems (DDS) due to its transformative potential in the field. FDF can be thought of as an extension of the well-established hot melt extrusion (HME) process, with the added advantages associated with AM: rapid prototyping; high spatial resolution; digital precision; and complex geometries attainable and integrable with other technologies, such as medical imaging techniques.[1] These advantages allow the fabrication of personalized DDS, which is sought after in the biomedical field,[1] including the pharmaceutical industry subsequent to the Precision Medicine Initiative in 2015.[2] For the pharmaceutical field, the advantages include dose flexibility, improved patient compliance, rapid administration, and improved medicine access.[3] FDF affords researchers the opportunity to reduce their laboratory footprint and resource expenditure as a number of devices can be printed, including tablets,[4] capsules,[5] transdermal microneedles,[6] catheters,[7] and topical masks.[8] Furthermore, the drug dissolution properties can be altered without requiring further tools. For example, where pore formers or freeze drying for traditional fabrication techniques was required to incorporate porosity into DDS, this can be seamlessly achieved by FDF without the need for additional materials or equipment.[9] In comparison to HME, different shapes are attainable without the need for multiple dies, which incidentally produces a fixed cross-sectional geometry that unavoidably spans the length of the extrudate. It has been stated that the short-term prospects are likely to lie within early-phase drug development as three-dimensional (3D) printing integration is likely to be attainable under current regulatory pathways.[3] An FDF printer compliant with current good manufacturing practices has been recently built, and the related processing conditions and product quality parameters were also reported.[5] The printer was used to fabricate multicompartmental capsular systems that were originally devised for personalized dosages. Goyanes et al. studied the in vivo behavior of 3D printed drugs in rodents.[10] Research into dosage forms of varying geometries and sizes for improved gastric emptying properties surmised that 3D printing could facilitate preclinical testing of new drug candidates in animal

Received: November 2, 2018
Accepted: February 19, 2019
Published: March 18, 2019

© 2019 American Chemical Society

DOI: 10.1021/acsomega.8b03057
ACS Omega 2019, 4, 5412−5423

models. The study also concluded that 3D printing was capable of printing solid dosage forms and variation in designs thereof affects disintegration in rodent models. Suffice it to say, the state-of-the-art technology is relatively new and requires concerted, multidisciplinary research to realize its full potential for fabricating DDS.

To date, research has been undertaken to understand the key processing facets of 3D printing. Nasereddin et al. used principal component analysis to predetermine filament suitability for FDF during the feeding process. Using a texture analyzer to simulate the forces a filament exhibits during feeding, the researchers demonstrated a method to accurately distinguish between feedable and nonfeedable filaments.[11] Zhang et al. analyzed different drug-containing filaments consisting of different polymers and experimentally determined that the ideal breaking stress should be above 2941 g/mm^2 and breaking distance should be above 1 mm, to achieve optimal feeding and printing conditions.[12] Kollamaram et al. further expanded the possibilities of FDF by demonstrating that temperatures as low as 90 °C can be used to print thermolabile drugs, such as Ramipril, by using Kollidon.[13] The choice of polymer can be exploited to alter the release profile of quinine,[14] and polymers that have been investigated via FDF thus far include polylactide (PLA), polycaprolactone (PCL), Kollidon, Eudragit, poly(vinylpyrrolidone), poly(vinyl alcohol), and hydroxypropyl methylcellulose.[15] Furthermore, both organic and inorganic additives have been incorporated to alter the printing performance of the filament, including its thermal, mechanical, and rheological properties.[16]

A number of studies have incorporated plasticizers to facilitate the processing of their DDS via FDF, thereby illustrating the indispensability of plasticizers. However, the studies did not provide experimental evidence regarding the effects of plasticizers and their relevance to FDF processing.[4,13,16−19] Okwuosa et al. relied on differential scanning calorimetry (DSC) to deduce whether their polymeric system was affected by a plasticizer; however, this only provides the evidence of plasticization as a function of temperature but not shearing,[20] given that both temperature and shearing occur in FDF. Therefore, to complement studies performed in this field, which have focused on aspects such as shape design,[4] dose adjustment,[21] drug-release characteristics,[22] and assessing the feasibility of polymers for FDF,[14,23] an original rheological and mechanical perspective was provided on the effect of plasticizers on processing facets pertinent to FDF. Identifying suitable plasticizers, and the amount thereof, is important; however, establishing validation methods to predict the printability of filaments has thus far focused on assessing their mechanical properties.[7]

As with traditional fabrication techniques, rheology is a key aspect of FDF processing, yet it remains underutilized. Rheology allows for analyses to be performed that can be correlated to the processing performance of melt-based fabrication techniques[24] and thereby preclude the need for time-consuming and costly empirical trials. Rheological analyses have also been used to interpret the polymeric structure of melts.[24] FDF is a relatively new technology in pharmaceutics, and thorough rheological investigations are still needed to predict material performance. For example, although FDF is an extension of HME, the mode of shearing differs between the two technologies, and thus viscosities suitable for HME may not be suitable for FDF. Moreover, the processing speed and the layer-by-layer approach to three-dimensional shaping suggest that the tolerance for expansion and shrinkage caused by the viscoelastic properties thereof following extrusion may be different from that of HME and other traditional melt fabrication techniques. Adhesion to a substrate is also an important aspect of FDF, which is in contrast to conventional fabrication techniques where it was considered undesirable.[25−27] On the contrary, FDF requires the initial deposited layer to form an adhesion to a preferably heated build plate with sufficient structural integrity to establish a foundation for subsequent layers to be deposited.[28] The layer to adhere to is required to resist detachment from the build plate while either the build plate or nozzle travels. Therefore, FDF presents new rheological and mechanical facets that require elucidation to facilitate DDS processing and mitigate processing failures (Figure 1).

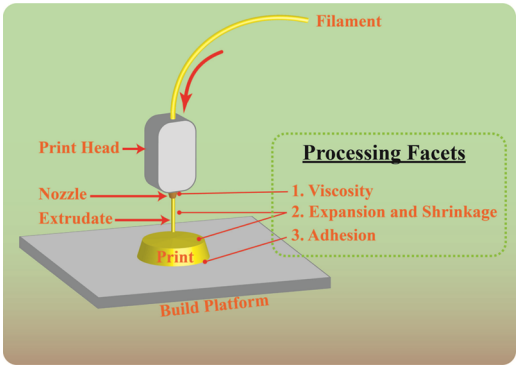

Figure 1. Schematic of the fused deposition fabrication technique. The illustration highlights rheological and mechanical facets of interest that will be investigated herein.

The effect of different molecular weight poly(ethylene glycol) (PEG) on polycaprolactone (PCL) loaded with ciprofloxacin (CIP) was investigated. PEG has been previously used as a plasticizer to address processing issues in other fabrication techniques, primarily the viscosity.[29] The effect of PEG and different molecular weights thereof has hitherto not been examined for FDF. It was hypothesized that plasticization, in addition to affecting viscosity, would also impact the solidification and adhesive qualities, which have not been investigated for FDF. In this article, the effect of PEG on the viscosity, solidification, and adhesive characteristics of PCL-CIP blends was examined.

2. RESULTS

2.1. Viscosity Measurement of PCL-CIP-PEG Filaments. Filament complex viscosity was measured at 130, 150, and 170 °C, and the results are presented in Figure 2. The formulations were found to be shear-thinning across all three temperature points, wherein an increase in angular frequency (ω) (i.e., shearing rate) decreased the viscosity. At 130 °C, neat PCL (nPCL) exhibited Newtonian plateau on the order of 10^4 Pa s, until 1.7 rad/s, after which it began to decrease notably and reached a viscosity of 10^3 Pa s. The addition of 20% w/w CIP decreased the complex viscosity of PCL, with an initial viscosity on the order of 10^3 Pa s, which is calculated to be a decrease of 39%. The addition of 10% w/w PEG 200 into PCL-CIP further decreased the viscosity; the initial viscosity, which was also on the order of 10^3 Pa s, decreased 76%. Increasing the content of PEG 200 to 15% w/w had a marked

DOI: 10.1021/acsomega.8b03057
ACS Omega 2019, 4, 5412−5423

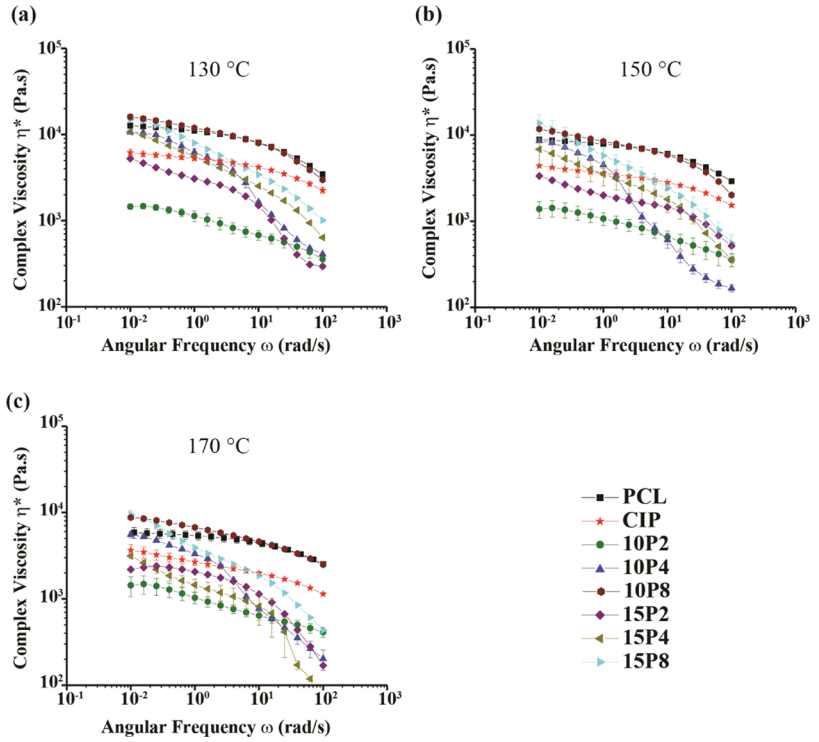

Figure 2. Complex viscosity for all of the filaments at (a) 130, (b) 150, and (c) 170 °C ($n \geq 6$).

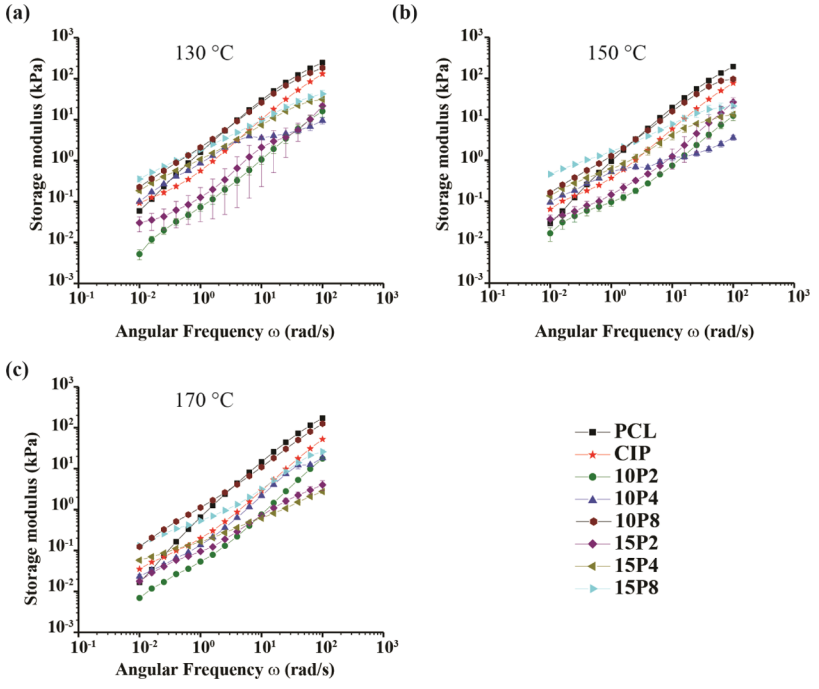

Figure 3. Storage modulus for all of the filaments at (a) 130, (b) 150, and (c) 170 °C.

increase on the viscosity initially; however, the viscosity was comparable to that of PCL-CIP-10P2 at 10^2 rad/s. Compared to PCL-CIP, the initial decrease in viscosity was 14%; however, PCL-CIP-15P2 showed markedly more shear-thinning than the binary blend. PCL-CIP-10P4 was found to have an initial complex viscosity on the order of 10^4 Pa s, an increase of 73% in comparison to PCL-CIP. The sample did not present with an evident Newtonian plateau, and hence was shear-thinning from the outset to the extent that it possessed a final value on the order of 10^2 Pa s, 1 order of magnitude lower than that of PCL-CIP. Similar results were found for PCL-CIP-15P4, PCL-CIP-10P8, and PCL-CIP-15P8, for which the initial viscosities were greater than the binary blend, by 74, 161, and 143%, respectively; however, the final viscosity was lower than that of PCL-CIP. Moreover, PCL-CIP-10P8 and -15P8 possessed initial viscosities greater than that of nPCL, by 26 and 17%, respectively.

DOI: 10.1021/acsomega.8b03057
ACS Omega 2019, 4, 5412−5423

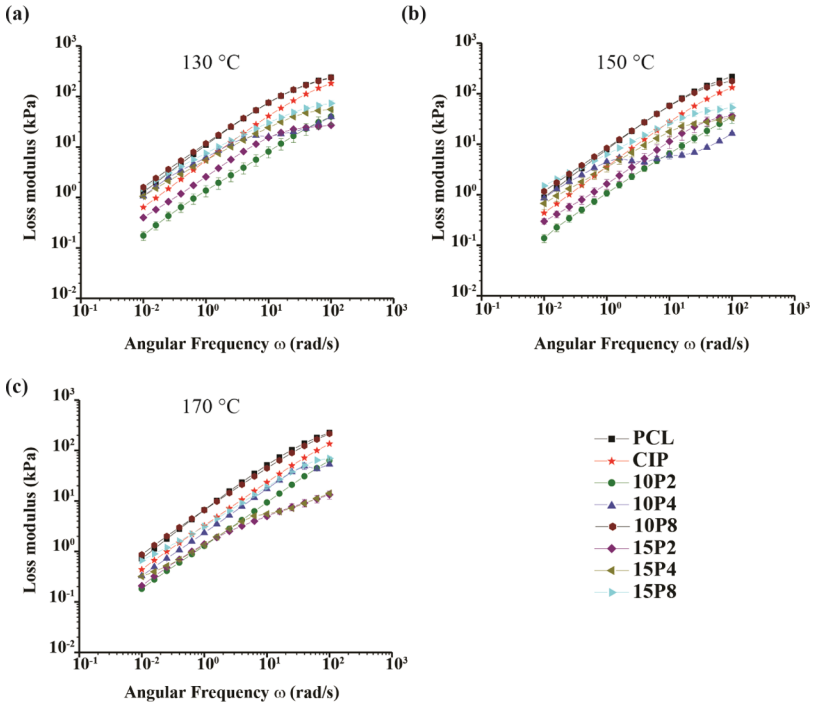

Figure 4. Loss modulus for all formulations at (a) 130, (b) 150, and (c) 170 °C.

Increasing the temperature resulted in a decrease in viscosity for all of the filaments. For example, the complex viscosity of nPCL decreased by 30 and 54%; PCL-CIP decreased by 28 and 41%; PCL-CIP-10P2 decreased by 5 and 2%; and PCL-CIP-15P8 decreased by 8 and 36%, at 150 and 170 °C, respectively. Similar changes as a result of incorporating CIP and CIP with PEG into nPCL were found at both 150 and 170 °C to that observed at 130 °C. The incorporation of CIP into nPCL reduced its viscosity between the measured frequency range, a decrease of 50 and 51% for 150 and 170 °C, respectively. The addition of PEG 200 further reduced the viscosity. At 150 °C, both PEG 4000 and 8000 increased the initial viscosity of PCL-CIP but were again more shear-thinning than PCL-CIP and exhibited lower viscosities at higher angular frequencies. Again, the addition of PEG 8000 was found to yield an initial viscosity greater than that of nPCL at 150 and 170 °C. Increases of 32 and 49% at 150 and 170 °C, respectively, were observed for PCL-CIP-10P8 compared to nPCL, and increases of 54 and 61% at 150 and 170 °C, respectively, were observed for PCL-CIP-15P8. At 170 °C, PCL-CIP-15P4 was found to possess lower viscosities than PCL-CIP across the investigated angular frequency range, with the difference further increasing as the angular frequency increased. Thus, different molecular weights of PEG, and varying content thereof, produced different results at different temperatures. In general, it can be summarized that the addition of both 10 and 15% w/w PEG 200 synergistically plasticized PCL, along with CIP, whereas PEG 4000 and 8000 were found, in all but one case, to increase the initial viscosity, but due to being more shear-thinning, the increase in viscosity was limited to low shear rates.

For insight into the microstructures of nPCL and PCL blends, the storage modulus (G') and loss modulus (G'') were also investigated, and the results are portrayed in Figures 3 and 4, respectively. The results demonstrated that with increasing angular frequency, the G' increased. It was discovered that PCL-CIP and the ternary blends with 10P4, 15P4, 10P8, and 15P8 possessed an initially greater storage modulus than nPCL, with the latter possessing a value 1 order of magnitude greater than nPCL. However, the increase in G' as a result of the incorporation of the said components was reversed at higher angular frequencies, whereby at 10^1 rad/s, nPCL possessed the greatest storage modulus until the end of the test. PCL-CIP-15P2 possessed an initial value comparable to nPCL, except for at 130 °C, where it was lower. For PCL-CIP-10P2, the entire profile, including the initial value, 2 was lower than that of nPCL. Therefore, the data highlighted that the higher-molecular-weight PEG temporarily increased the storage modulus in comparison to nPCL, whereas PEG 200 either had no initial effect or reduced the storage modulus.

The loss modulus was also found to increase with increasing angular frequency for all samples. At 130 °C, PCL-CIP was found to possess a lower G'' than nPCL. The G'' further decreased with the addition of PEG 200 across all angular frequencies, and was observed also at 150 and 170 °C. Conversely, PEG 4000 and 8000 exhibited an initially greater value that was eventually surpassed by PCL-CIP at higher shearing rates. At higher temperatures, the initial gain of PEG 4000 was found to decrease, while at 170 °C, PCL-CIP exhibited a G'' greater than PCL-CIP-10P4 and PCL-CIP-15P4 throughout the measured range. PCL-CIP-15P8 maintained an initial G'' comparable to that of nPCL at 150 and 170 °C, and similarly to that at 130 °C, G'' was greater for nPCL with increasing angular frequency. PCL-CIP-10P8 initially possessed a greater loss modulus than nPCL but was comparable by the end of the test. Hence, in contrast to the storage modulus data, none of the blends exhibited a loss modulus value notably greater than nPCL at low angular frequencies.

2.2. Rheological Stability of Filaments. A time ramp at 170 °C was performed to determine the rheostability of the samples, and the results are presented in Figure 5. The analysis

DOI: 10.1021/acsomega.8b03057
ACS Omega 2019, 4, 5412−5423

confirmed that the samples were stable for 5 min. The implications of this result, for both rheological analyses and 3D printing, are discussed in Section 3.

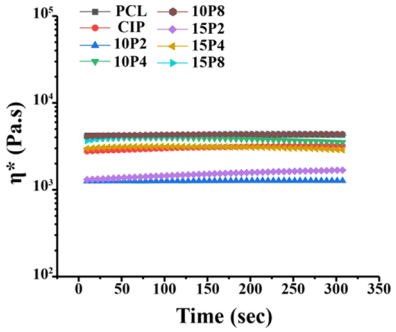

Figure 5. Time ramp performed at 170 °C, with strain and frequency of 0.1% and 10 rad/s, respectively ($n \geq 3$).

2.3. Viscoelastic Changes of PCL-CIP-PEG during Cooling. Following extrusion, the extrudate was deposited onto a heated build plate, in which the material undergoes cooling and consequently solidification. To determine the effects of CIP and PEG on PCL during this stage, dynamic cooling ramps were performed to examine the elastic behavior thereof. Figure 6 displays the storage modulus, loss modulus, and tan δ when cooled from 170 to 40 °C, which corresponded to the nozzle temperature and build plate temperature, respectively. The cooling ramps were performed following the shear test performed as shown in Figure 2 at 170 °C. The storage modulus (G') is the elastic component of materials, and as Figure 6a demonstrates, the G' of all samples increased exponentially as the temperature decreased. PCL possessed the highest G' throughout the cooling ramp, and the rate thereof increased once the temperature was below 100 °C. The addition of CIP reduced the elastic component of PCL, with a similar exponential rise detected. The addition of PEG 200 reduced the elastic component of PCL-CIP, and the exponential increase in G' was markedly less pronounced. Alternatively, the inclusion of PEG 4000 resulted in comparable increases in G' to that of PCL-CIP, whereas a considerable rise in G' was observed with the inclusion of PEG 8000 into PCL-CIP, albeit the G' was comparable at 160 °C. Table 1 presents the decrease in moduli at the start and end of the G' test of the PCL blends in comparison to neat PCL. As enumerated, the difference in G' was lower at the end of the test (40 °C) than at the start of the test.

Table 1. Percentage Difference in Moduli with Respect to Neat PCL at the Start and End of the Cooling Ramp[a]

	% decrease in moduli			
	G'		G''	
sample	start	end	start	end
PCL				
PCL-CIP	83.2	49.7	61.7	19.3
PCL-CIP-10P2	95.4	82.6	84.2	60.0
PCL-CIP-10P4	83.8	49.7	66.6	25.8
PCL-CIP-10P8	42.7	8.5	27.3	+5.7
PCL-CIP-15P2	87.9	86.9	74.5	75.3
PCL-CIP-15P4	92.5	46.1	85.8	26.1
PCL-CIP-15P8	72.8	23.5	61.4	10.9

[a]All results represent a percentage decrease unless preceded by a "+", which denotes a percentage increase.

A similar profile in the loss modulus was observed in all of the samples, whereby cooling of the filaments to between 100 and 120 °C resulted in an exponential increase in the modulus thereafter (Figure 6b). PCL-CIP-10P8 possessed the greatest G'', which was followed by neat PCL and PCL-CIP-15P8. The lowest G'' was again observed in the blends containing PEG 200. In comparison to the storage modulus, the loss modulus

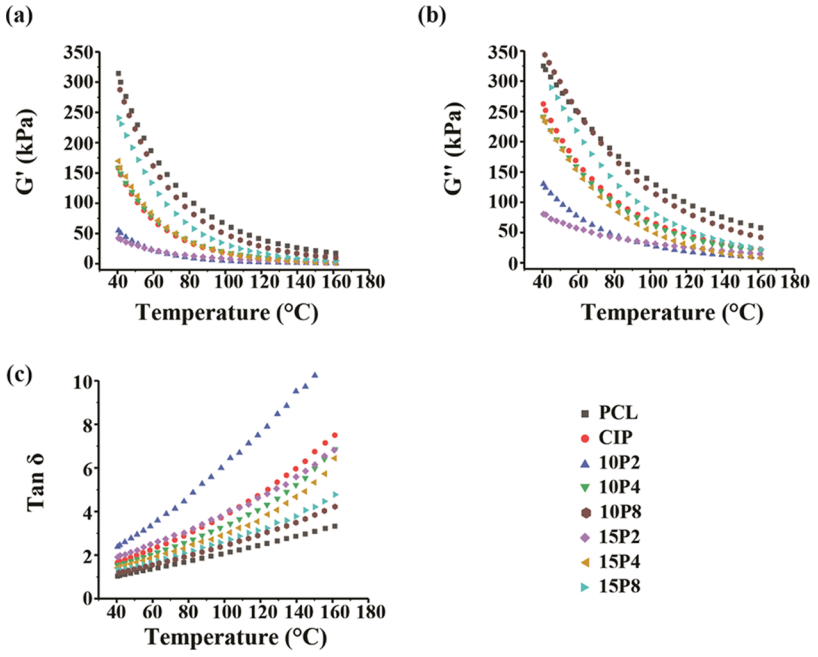

Figure 6. Viscoelastic measurements of the filaments performed when cooled from 170 to 40 °C. All samples were presheared from 0.1 to 100 rad/s prior to analysis. (a) Storage modulus, (b) loss modulus, and (c) tan δ ($n \geq 3$).

DOI: 10.1021/acsomega.8b03057
ACS Omega 2019, 4, 5412−5423

of PCL was affected to a lesser extent. Table 1 presents the decrease in both moduli of the PCL blends with respect to neat PCL. The results revealed that the percentage decrease in the storage modulus was greater than that of the loss modulus. Nonetheless, the incorporation of CIP and CIP with PEG affected the elastic and viscous components of PCL.

Figure 6c illustrates the tan δ results obtained during cooling, which is the ratio between the loss modulus and storage modulus. Values above and below 1 indicate that a sample is predominantly viscous and predominantly elastic, respectively. The data revealed that the tan δ values decreased for all samples with decreasing temperature between 170 and 40 °C and were approaching 1. Neat PCL had a tan δ value of 1.0 at 40 °C when rapidly cooled; thus, it transitioned from a predominantly viscous material to a solid in the probed range. PCL-CIP had a tan δ value of 1.7: the addition of 10 and 15% w/w PEG 200 resulted in values of 2.4 and 1.9, respectively; the addition of 10 and 15% w/w PEG 4000 resulted in values of 1.5 and 1.4, respectively; and the addition of 10 and 15% w/w PEG 8000 resulted in values of 1.2 and 1.3, respectively. Thus, the addition of CIP into PCL retarded its ability to solidify when cooled to 40 °C, but the discrepancy was minimized through the addition of higher-molecular-weight PEG. Despite only neat PCL achieving a predominantly solid state upon reaching 40 °C, it should be highlighted that the gradient of the PCL blends was markedly higher than that of neat PCL. In other words, the rate of solidification was greater in PCL blends, as Table 2 delineates.

Table 2. Slope of the tan δ Values of the Different Formulations[a]

sample	slope	% increase of slope over neat PCL	R^2
PCL	0.0187		0.99
PCL-CIP	0.0465	149	0.98
PCL-CIP-10P2	0.0743	297	0.99
PCL-CIP-10P4	0.0407	118	0.97
PCL-CIP-10P8	0.0246	32	0.99
PCL-CIP-15P2	0.0390	109	0.99
PCL-CIP-15P4	0.0316	70	0.95
PCL-CIP-15P8	0.0272	45	0.99

[a]The percentage increase over neat PCL is also included to illustrate that the blends had a larger gradient and thus exhibited a higher rate of solidification.

Polymer melts are susceptible to expansion. Moreover, the transition from high temperature to room temperature induces internal stresses that manifest into the material shrinking. The said behavior results in temperature-induced warpage, whereby the material contracts, and in the context of FDF, can result in the print de-adhering from the build plate. Warpage is a concern in FDF, particularly for large prints, which can result in failed prints. The rheometer employed in this study is equipped with axial motion and sensors, which were utilized to measure the expansion and subsequent shrinkage.

In simulating the events as the filament exits the nozzle, the expansion was measured while the temperature was rapidly reduced from 170 to 40 °C, and the results are portrayed in Figure 7. Neat PCL was found to undergo the largest expansion, peaking at 4.7 ± 0.4%, and followed by shrinkage. PCL-CIP-15P8 exhibited the second largest expansion peaking at 3.6 ± 0.5%, and followed by shrinkage. PCL-CIP had the third largest expansion at 2.5 ± 0.4%, followed by PCL-CIP-15P4 and PCL-CIP-10P4 at 2.5 ± 0.06 and 1.5 ± 0.03%, respectively. PCL-CIP-10P8 possessed a maximum shrinkage of 1.41 ± 0.15%. The inclusion of PEG 200 resulted in the smallest expansion of 1.5 ± 0.007 and 1.2 ± 0.006% for 15 and 10% w/w PEG 200, respectively. In addition, and apart from PCL-CIP-15P8, the onset of shrinkage started at lower temperatures compared to neat PCL. Therefore, the addition of CIP and PEG affected the maximum expansion that PCL underwent, as well as the onset thereof.

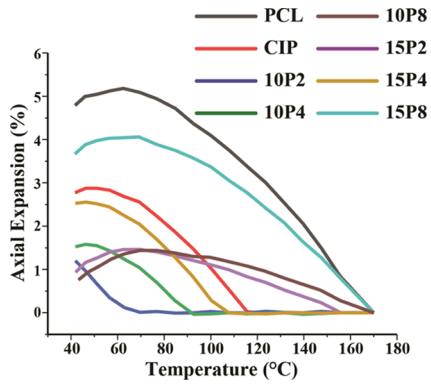

Figure 7. Expansion of filaments measured as a function of temperature during the cooling ramp ($n \geq 3$).

The shrinkage behavior of samples was also analyzed with a dwell time of 5 min. The analysis revealed that all of the samples had a tendency to shrink at 40 °C, as depicted in Figure 8. During the isothermal test, neat PCL did not shrink until after 169 ± 1 s, with a maximum shrinkage of 1.7 ± 0.1%. PCL-CIP-15P2 exhibited a similar delayed shrinkage, whereby shrinkage occurred after 222 ± 7 s, and a maximum of 0.8 ± 0.2% shrinkage was recorded. PCL-CIP-10P2 was found to initially increase by 0.2 ± 0.03% for the first 108 ± 8 s, followed by shrinkage of 3.5 ± 0.2%, thus giving a total shrinkage of 3.7%. For the binary blend of PCL-CIP, the shrinkage commenced after 33 ± 0.5 s and proceeded until the end of the test, with a maximum of 4.9 ± 0.1% shrinkage. Similar profiles were observed for PCL-CIP-10P4, -10P8 -15P4, and -15P8, with maximum shrinkages of 4.5 ± 0.01, 4.2 ± 0.12, 4.3 ± 0.05, and 4.8 ± 0.20%, respectively. Hence, the addition of CIP induced a greater axial shrinkage in PCL, and the addition of different PEG reduced the maximum linear shrinkage by different amounts.

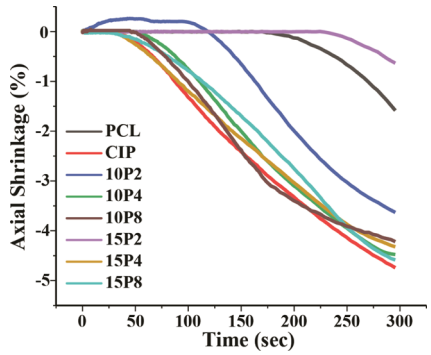

Figure 8. Axial shrinkage measured at 40 °C following the cooling ramp ($n \geq 3$).

2.4. Adhesive Properties of PCL-CIP-PEG Following Shearing. Once deposited onto a heated build plate, the

DOI: 10.1021/acsomega.8b03057
ACS Omega 2019, 4, 5412−5423

extrudate should adhere thereto and form a foundation for subsequent layers until the layer-by-layer process is complete. For this reason, the adherence characteristics were also measured using the tack function of the rheometer at 40 °C, following shearing at 170 °C to simulate FDF. The adhesion results are illustrated in Figure 9. If the debonding curve has an

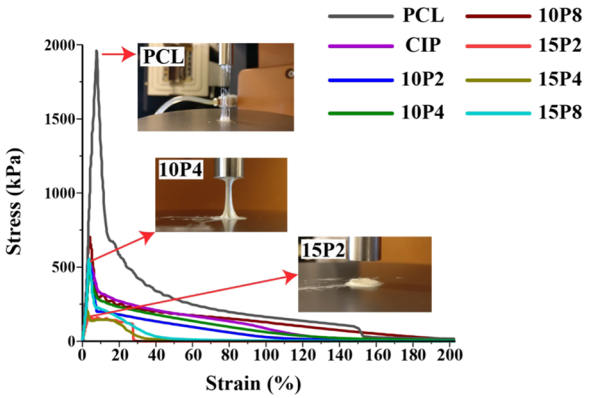

Figure 9. Adhesive test performed using the rheometer. All samples were presheared from 0.1 to 100 rad/s at 170 °C, cooled to 40 °C, and subsequently analyzed for their adhesive properties ($n \geq 3$).

equal increase and decrease in force, then the locus of material failure is at the interface (i.e., adhesive failure). Alternatively, if a gradual decrease follows the abrupt rise in stress, then the failure is said to be both adhesive and cohesive. Adhesion is the tendency of different materials to bond together, whereas cohesion is the tendency of similar materials to form a bond.[30]

The test revealed that the formulated neat PCL filaments were capable of adhering at 40 °C, with a peak yield stress of 1959 ± 82 kPa. The shape of the curve was asymmetrical, which is indicative of cohesive failure. The addition of CIP considerably reduced the maximum adhesive force to 539 ± 14 kPa, but the graph remained asymmetrical. Similar profiles was observed for PCL-CIP-10P2, -10P4, and -10P8 with peak forces of 581 ± 5, 468 ± 3, and 773 ± 56, respectively. The peak adhesive force decreased when the PEG content increased to 15% w/w, resulting in PCL-CIP-15P2, -15P4, and -15P8 exhibiting values of 166 ± 3, 229 ± 6, and 613 ± 19 kPa, respectively. Moreover, the curve of PCL-CIP-15P2 exhibited an abrupt decrease, which was indicative of adhesive failure.[31,32] The photograph inset of PCL-CIP-15P2 in Figure 9 exemplifies the lack of adhesion bonding. The test was repeated for PCL-CIP-15P2 with a dwell period of 10 min at 40 °C, and in another separate test where the preshearing was removed; however, both had an unremarkable effect and the sample maintained its adhesive failure (data not included). The analysis demonstrated that the addition of CIP and PEG considerably reduced the peak adhesive force of PCL, with further decreases observed in PCL-CIP-15P2 and 15P4. Finally, only PCL-CIP-15P2 failed in a solely adhesive manner.

3. DISCUSSION

Ternary blends of polycaprolactone, ciprofloxacin, and poly(ethylene glycol) of different molecular weights were successfully fabricated using a hot melt extruder, which were intended for 3D printing using a fused deposition fabrication technique. PEG was incorporated to modify the characteristics of the drug device, and in this paper, the effects thereof with respect to rheology and mechanical characteristics were investigated. A subsequent publication will report on the FDF findings. Rheology is an indispensable tool that can facilitate understanding the effect of formulation on processing[33] and elucidating the drug−polymer miscibility,[34] as well as serve as prefigure to the tensile properties of polymers.[35]

To the author's best understanding, rheological analyses performed in the field of FDF and pharmaceutics have solely focused on the effect of formulation on viscosity.[36−39] This is indeed important and is the first rheological event encountered in FDF. A previous work by Boetker et al. has found complex viscosities on the order of 10^3 and 10^4 Pa s to be suitable for FDF printing,[37] which is similar to this work. Holländer et al. found viscosities on the order of 10^3 Pa s when measured using steady-state shearing.[38]Steady-state and dynamic-state shearings are comparable provided that the Cox−Merz rule is applicable, and it will be discussed in the following publication.

Previous research has reported indomethacin to decrease the viscosity of PCL,[38] and the present study confirmed CIP to have a similar effect. The data revealed the degree of plasticization by CIP to be temperature-dependent, as a greater decrease in viscosity was observed in comparison to neat PCL at 150 and 170 °C than at 130 °C. Both the storage and loss moduli were examined to elucidate the changes in viscosity. The storage modulus is used to provide insight into polymer elasticity[24] and entanglement,[40] whereas the loss modulus is a reflection of the energy dissipated, such as that from molecular friction.[41,42] It was evident that the decrease in viscosity was due to a decrease in the loss modulus, in which chain slippage increased with the substitution of 20% w/w PCL for CIP. Interestingly, an increase in G' was observed at low ω, which is believed to be due to CIP agglomeration, effectively behaving as an inorganic filler in a polymer.[24] The deagglomeration thereof produced the inflection point delineated in G' (Figure 3) and thereafter presented with a similar slope to that of nPCL. Previous studies have found that increasing the filler content results in an increase in G' at low ω,[43−47] which is indicative of agglomeration.[43,44] Nevertheless, the initial increase in elasticity was insufficient to increase the viscosity of PCL-CIP at low ω. The viscosity data infer that lower extrusion pressures will be needed for PCL-CIP to flow in comparison to nPCL. Moreover, the decrease in loss modulus indicated no interaction between PCL and CIP (i.e., an immiscible system).[48] DSC data obtained by the author confirmed that it was an immiscible system (data not presented herein).

The incorporation of PEG 200 yielded the lowest viscosities, which was expected due to the proportional relationship between plasticizer molecular weight and viscosity.[49−51] Unlike the other PEGs, the temperature was sufficient in decreasing the viscosity in relation to PCL-CIP, whereas higher-molecular-weight PEGs required shearing in addition. The synergistic decrease in viscosity with the inclusion of PEG 200 was again evident from the viscoelastic data, as the addition thereof reduced both G' and G''. In contrast to the higher-molecular-weight PEG, PEG 200 reduced the level of entanglement of PCL-CIP and also increased the free volume of the melt, thereby effectively lubricating the chains,[52] and hence the lower G''.

At lower shearing rates, PCL-CIP-10P4 and -15P4 exhibited viscosities greater than PCL-CIP. The moduli data revealed that at lower frequencies, both G' and G'' were greater than that of PCL-CIP, thus demonstrating that PEG 4000 increased the system's stiffness and molecular friction as a result of the

DOI: 10.1021/acsomega.8b03057
ACS Omega 2019, 4, 5412−5423

polymeric system being immiscible. Except for at 170 °C, the viscosity of PCL-CIP-15P4 was lower than that of CIP, which again was due to the former possessing a lower G'' despite a greater G'. It can be deduced that G'' was a better determinant of complex viscosity than G'. Furthermore, the moduli results also revealed why only the viscosity of PCL-CIP-15P8 was greater than that of nPCL at lower frequencies, as it exhibited comparable G'', yet G' was greater by 1 order of magnitude at lower frequencies, across all temperature points. Herein, the increase in G' at low frequencies between PCL and PEG 4000 and 8000 was due to the relatively high-molecular-weight PEGs dispersed within PCL as droplets. Scanning electron microscopy (SEM) images of PCL-CIP-15P8 were compared to those of both nPCL and PCL-CIP, which confirmed that PEG 8000 was dispersed within PCL as droplets. The SEM images are provided in the Supporting information. An increase in G' at low frequencies is well known to be reflective of an immiscible system,[53] and has been previously ascribed to the excess stress exhibited at the interfacial region between the polymers.[54] This resulted in the blends thereof possessing higher shear-thinning characteristics. Previous studies have reported high-molecular-weight PEGs to be immiscible with PCL.[55−58] The effect of low-molecular-weight PEG on PCL observed herein was similar to that observed for polylactide (PLA), in which small PEG molecules capable of inserting between the PLA chains were better plasticizers. The time ramp confirmed that the decrease in viscosity for all blends was due to shearing and not time (Figure 5). Other causes of viscosity changes with respect to time include material degradation, which presents as rheopectic behavior; however, this was also not observed, and hence, it can be concluded that no significant degradation took place.

The advantage of reducing the viscosity allows printing to be performed at lower temperatures, which, for example, could allow thermally labile drugs to be printed using FDF that would otherwise degrade at high temperatures. However, a disadvantage of the viscosity being too low is that it could lead to premature seepage, given the orientation of the nozzle. In FDF, prior to extrusion, the nozzle is initially heated to the designated temperature while housing the filament. If the viscosity is too low, then the filament can begin to drip or flow before pressure is applied. This phenomenon is undesirable as it wastes material and could result in poor prints. Thus, from this study, PCL-CIP-15P8 was identified as a promising formulation as it possessed the highest viscosities at low shear rates, and yet at higher shear rates, it flowed similar to both neat PCL and PCL blends.

Following extrusion, the material is required to solidify to provide the structural integrity to support the deposition of ensuing layers. The moduli of all formulations were found to increase as the temperature decreased. This suggested the polymeric network for all exhibited recoverable deformation despite being presheared at large-amplitude oscillatory shear. The addition of CIP and CIP with PEG reduced the time it required for PCL to solidify, as only nPCL was predominantly solid, whereas PCL blends were still predominantly liquid by the end of the test. Thus, this study revealed that the addition of drug and PEG impacted the cooling dynamics of polymer melts and should be investigated in addition to the viscosity. The results suggest that a lower FDF processing speed may be required to ensure that the PCL blends solidify and prevent defects such as “elephant foot”, in which the upper layers press down on the foundation layer before it solidifies, consequently causing it to protrude.[59]

This study further revealed that the expansion and shrinkage the different materials underwent during cooling having been subjected to a preshear. Shrinkage is caused by thermal contraction as the material is rapidly cooled by the large thermal gradient of the surrounding air.[60] It was concluded that the addition of CIP and PEG reduced the tendency of PCL to expand, which again is related to their storage and loss moduli. The incorporation of CIP and PEG increased the tendency of the PCL to shrink at 40 °C. This is due to the longer cooling times required for the PCL blends, as longer cooling times give higher mobility to molecular chains to form crystalline structures and thus the higher shrinkage.[61] Previous work on injection molding reported an increase in thermoplastic starch shrinkage percentage difference when glycerol, the plasticizer, content was increased from 10 to 18 wt %.[62] Thus, the effect of chain mobility through plasticization should be considered during cooling, in addition to its desired effect on extrusion flow. Indeed, a thermal mechanical analyzer could be utilized to determine the level of expansion or shrinkage exhibited by the polymer, but the added benefit of the approach proposed herein is that the rheometer allows for a preshearing, hence providing a better reflection of the events occurring in FDF. A significant dimensional change could lead to warpage,[60] and the residual stress that causes shrinkage can also affect the mechanical properties[63] of the solidified print; hence, characterizing dimensional changes can aid in the preempting of processing issues. PCL-CIP-15P2 produced the least recorded shrinkage, but this is believed to be erroneous due to its inability to adhere to the rheometer, as determined by the adhesive test (Figure 9), and hence, the shrinkage thereof was not detected by the sensor.

The final stage of filament deposition ensures that the material adheres to the build plate. This study revealed that although the addition of CIP and PEG reduced the adhesive force of nPCL, a significant adhesion was maintained, except for PCL-CIP-15P2, which failed in an adhesive manner.[31] Adhesive failure is undesirable as it suggests that the material is unlikely to adhere to the build plate and thereby unable to establish a foundation layer for the print. Previous works have noted that higher printing speeds, and therefore higher shear rates, caused a decrease in adhesion strength,[30] and for that reason, PCL-CIP-15P2 was retested without any preshear, but adhesion failure was once again observed. In addition, to see whether more time was needed for the macromolecules of the polymer to adhere to the build plate, a dwell time of 10 min was incorporated prior to the adhesive test, but again adhesion was not observed. Therefore, although plasticization of melts is regularly sought after for improving flow behavior, considering the adhesive consequence thereof.

The decrease in adhesive strength in PCL-CIP is likely to be due to the low solubility between the two materials.[64,65] Previous works on transdermal patches have reported a decrease in adhesive forces as a result of drug incorporation.[66] For example, Gullick et al. found that increasing the amount of captopril above 13% w/w reduced the work of detachment of bioadhesive polymers.[67] Michaelis et al. reported that an ibuprofen concentration above 1% reduced the adhesiveness of their polymer.[68] The addition of higher-molecular-weight polymers did not significantly affect the maximum peak stress of PCL-CIP, except for when PEG 4000 was increased from 10 to 15% w/w. A notable decrease in adhesiveness was also

DOI: 10.1021/acsomega.8b03057
ACS Omega 2019, 4, 5412−5423

Table 3. Sample Names and Respective Mass Compositions

	composition (% w/w)				
			poly(ethylene glycol)		
sample name	polycaprolactone	ciprofloxacin	PEG 200	PEG 4000	PEG 8000
nPCL	100	0			
PCL-CIP	80	20			
PCL-CIP-10P2	70	20	10		
PCL-CIP-15P2	65	20	15		
PCL-CIP-10P4	70	20		10	
PCL-CIP-15P4	65	20		15	
PCL-CIP-10P8	65	20			10
PCL-CIP-15P8	65	20			15

observed when the addition of PEG 200 was increased from 10 to 15% w/w. Repka and McGinity found PEG to decrease the adhesion strength of hydroxypropylcellulose hot-melt-extruded films containing polycarbophil.[69] They postulated that many of the reactive sites available to form adhesion to their substrate were occupied by PEG, thereby decreasing the adhesive properties. Fisher and Rowe (1976) also recorded a decrease in adhesion force in hydroxypropyl methylcellulose films when propylene glycol was increased from 10 to 20%.[70] Rowe (1976) reported that as the molecular weight of PEG decreased, the mole fraction of interactive hydroxyl group increased.[71−73] Accordingly, PCL-CIP-15P2, possessing the lowest-molecular-weight PEG and at the highest concentration thereof, may have saturated the available sites for bonding to the substrate to the extent that the blend could not form an adhesion thereto. Moreover, PEG 200 has been reported to display preferential movement toward the top surface of polymer compared to other plasticizers.[74] Considering that PEG 200 is more volatile than PEG 4000 or 8000, its movement to the surface may have been expedited when subjected to high temperatures. Consequently, as a liquid PEG at room temperature, unlike PEG 4000 and 8000, which are solid PEGs, it may have lubricated the surface of PCL and thereby prevented adhesion.

In summary, from an FDF perspective, PEG 8000 was determined as the ideal viscosity modifier for the present polymeric system. PEG 8000 provided high viscosity at low shear rates but was strongly shear-thinning; was found to exhibit a lower tan δ when cooled from 170 to 40 °C than PCL-CIP; and exhibited a higher adhesion peak stress than PCL-CIP while maintaining adhesion to a dissimilar substrate. These qualities suggest that PCL-CIP-10P8 is the most stable ternary blend at high temperatures, yet can flow with increasing shear, can solidify quicker and thus improve the processing speed over PCL-CIP, and can adhere to the heated build plate, thereby establishing a foundation layer for the print. The incorporation of PEG 4000 was found to be the second most effective excipient when considering the aforementioned criteria. PEG 200 was found to be the least-compatible additive for PCL-CIP, with a limited FDF processability of 10% w/w.

4. CONCLUSIONS

In fused deposition fabrication, filaments are required to flow at high temperature, solidify rapidly, and adhere to the build plate. In this work, the said processing facets were investigated. A rheometer was used to measure the complex viscosity and viscoelastic properties during cooling. The results demonstrated that a binary blend of PCL and CIP was found to possess a lower viscosity, increase the time needed for solidification, and decrease the adhesion strength, in comparison to neat PCL. The addition of PEG produced different responses depending on the molecular weight. PEG 200 was found to augment the effect of CIP by further reducing the viscosity and increasing the solidification time. Regarding the adhesive strength, the incorporation of 15% w/w PEG 200 produced a blend that failed in an adhesive manner. The inclusions of PEG 4000 or 8000 was a better excipient candidate for FDF, and the addition of 10% w/w PEG 8000 yielded filaments that were desirably more shear-thinning, solidified quicker, and enhanced the peak adhesion strength in comparison to PCL-CIP. The essence of the article illustrated that processing aspects other than viscosity should be measured to determine formulation suitability for FDF and that different molecular weights of PEG produced distinct effects on the viscosity, cooling, and adhesive properties of PCL-CIP.

5. EXPERIMENTAL SECTION

5.1. Raw Materials. Polycaprolactone (M_n = 80 000 g/mol), acetic acid (96%), ciprofloxacin (98.0%), and poly(ethylene glycol) (PEG, M_w = 4000 and 8000 g/mol) were purchased from Sigma-Aldrich Chemie GmbH (Steinheim, Germany, and St. Louis). Poly(ethylene glycol) (M_w = 200 g/mol) was obtained from Fluka. Acetone (≥99.5%) was purchased from VWR (France), and dichloromethane (DCM) was purchased from Fisher Scientific (Germany). All chemicals were used without further purification.

5.2. Fabrication Process of Drug-Delivery Device. *5.2.1. Solvent Casting.* The drug-loaded PCL films were initially blended using solvent casting to facilitate mixing. First, PCL granules were dissolved in DCM at room temperature to prepare PCL solutions with different concentrations. Then, PEG was added to the solution and stirred for 5 min. Ciprofloxacin solution was prepared separately by adding 1 g thereof to 10 mL acetone and adjusting the pH of solution to 3 using acetic acid. Both the ciprofloxacin and PCL solution were then mixed and stirred for 5 min. The solutions were cast on dust-free Petri dishes, which were covered with a lid, and the solvent was allowed to evaporate in ambient conditions and at room temperature for 3 days. The films contained 20% w/w drug and different amounts of PEG and PCL. Samples were named based on the composition and percentage and molecular weight of PEG, and are delineated in Table 3.

5.2.2. Hot Melt Extrusion. A 5 cc twin screw extruder (DSM Xplore, the Netherlands) was employed to generate the

DOI: 10.1021/acsomega.8b03057
ACS Omega 2019, 4, 5412−5423

filaments for FDF printing. The solvent-cast films were introduced to the HME and extruded using a temperature and a torque speed of 120 °C and 100 rpm, respectively, with a total circulation time of 3 min. The extrudates were cooled in ambient conditions. Examples of fabricated films are portrayed in Figure 10.

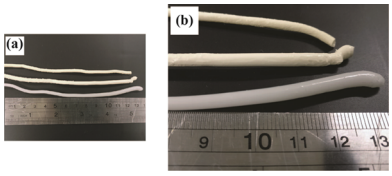

Figure 10. (a) Image depicting the filaments fabricated, with (b) a closer perspective to highlight the difference in color. The filament in the bottom row is of neat PCL (white color), the middle is of PCL-CIP, and the top is of PCL-CIP-15P8.

5.3. Rheological Characterization. The DHR2 (TA Instruments) was used for both rheological and mechanical analyses, with an 8 mm parallel plate geometry and an analysis gap of 0.5 mm. The Trios software that was provided by the manufacturer was used for both setting the parameters and analyses. All of the measurements began at high temperatures. Upon reaching the desired temperature, the sample was placed centrally onto the Peltier plate, and the upper geometry was lowered to the trimming gap of 0.55 mm. Any excess material was trimmed before the upper geometry was further lowered to the analysis gap. The test was immediately started once the analysis gap was reached. For Sections 5.3.3−5.3.5, where multiple procedures were used, the Trios software was used to write scripts that allowed one procedure to immediately commence following the previous procedure.

5.3.1. Oscillatory Frequency Sweep Test. The oscillation frequency tests were performed to obtain the complex viscosity as a function of frequency. Tests were conducted at 130, 150, and 170 °C, with a strain of 0.1% and an angular frequency (ω) range of 0.1−100 rad/s. The parameters were determined following an oscillatory amplitude sweep performed on PCL (i.e., control sample) to determine the linear viscoelastic region. The amplitude test was performed at 170 °C, with an angular frequency of 1 rad/s and a strain range of 0.01−1000%. The amplitude sweep revealed a yield in strain on the order of 10^0, and consequently, a strain of 0.1% was used to ensure that the frequency sweep measurements began in the linear viscoelastic region for the control sample.

5.3.2. Oscillatory Time Ramp. Time ramp measurements were performed at 170 °C for 5 min. A strain of 0.1% and an angular frequency of 0.1 rad/s were selected, which ensured that the tests were performed in the terminal region.

5.3.3. Oscillatory Cooling Ramps. For the cooling dynamics, samples were first sheared at 170 °C according to the above frequency sweep protocol (Section 5.3.1), after which the stage was cooled to 40 °C at 50 °C/min while the viscoelastic parameters were measured at a strain and angular frequency of 0.1% and 10 rad/s, respectively.

5.3.4. Expansion and Shrinkage Measurements. For measuring the expansion during cooling, samples were presheared at 170 °C using the protocol detailed in Section 5.3.1. The samples were then cooled from 170 to 40 °C at 50 °C/min with a strain and ω of 0.1% and 1 rad/s, respectively, all the while applying an axial compressive force of 0.1 N. The protocol was repeated for the shrinkage measurement, while at 40 °C, an axial tensile force of 0.1 N was applied until the end of the test, which was 300 s.

5.3.5. Adhesive Measurement. The samples were first presheared at 170 °C using the frequency sweep profile detailed in Section 5.3.1. The samples were then cooled thereafter from 170 to 40 °C at a rate of 50 °C/min, with a strain and angular frequency of 0.1 and 10 rad/s, respectively. Upon reaching 40 °C, the upper geometry was programmed to rise at a constant rate of 0.1 mm/s while recording the axial force. The torque was set to 0 μN m during the test.

■ ASSOCIATED CONTENT

Supporting Information

The Supporting Information is available free of charge on the ACS Publications website at DOI: 10.1021/acsomega.8b03057.

Scanning electron micrograph confirming that the addition of PEG 8000 resulted in an immiscible filament, and the experimental procedure thereof (PDF)

■ AUTHOR INFORMATION

Corresponding Author

*E-mail: elbadawi.moe@gmail.com.

ORCID

Mohammed Elbadawi: 0000-0003-1304-3686

Notes

The author declares no competing financial interest.

■ ACKNOWLEDGMENTS

The project was supported by the Kempe Foundation, Sweden (Grant no. SMK-1640). The author thanks Armin Kiani and Prof. Minna Hakkarainen for supplying the PCL filaments. He also thanks Dariush Nikjoo for providing the SEM images found in the Supporting Information.

■ REFERENCES

(1) Ricles, L. M.; Coburn, J. C.; Di Prima, M.; Oh, S. S. Regulating 3D-Printed Medical Products. *Sci. Transl. Med.* **2018**, *10*, No. eaan6521.

(2) Collins, F. S.; Varmus, H. A New Initiative on Precision Medicine. *N. Engl. J. Med.* **2015**, *372*, 793−795.

(3) Trenfield, S. J.; Awad, A.; Goyanes, A.; Gaisford, S.; Basit, A. W. 3D Printing Pharmaceuticals: Drug Development to Frontline Care. *Trends Pharmacol. Sci.* **2018**, *39*, 440−451.

(4) Scoutaris, N.; Ross, S. A.; Douroumis, D. 3D Printed "Starmix" Drug Loaded Dosage Forms for Paediatric Applications. *Pharm. Res.* **2018**, *35*, 34.

(5) Melocchi, A.; Parietti, F.; Maccagnan, S.; Ortenzi, M. A.; Antenucci, S.; Briatico-Vangosa, F.; Maroni, A.; Gazzaniga, A.; Zema, L. Industrial Development of a 3D-Printed Nutraceutical Delivery Platform in the Form of a Multicompartment HPC Capsule. *AAPS PharmSciTech* **2018**, *19*, 3343−3354.

(6) Luzuriaga, M. A.; Berry, D. R.; Reagan, J. C.; Smaldone, R. A.; Gassensmith, J. J. Biodegradable 3D Printed Polymer Microneedles for Transdermal Drug Delivery. *Lab Chip* **2018**, *18*, 1223−1230.

(7) Awad, A.; Trenfield, S. J.; Gaisford, S.; Basit, A. W. 3D Printed Medicines: A New Branch of Digital Healthcare. *Int. J. Pharm.* **2018**, *548*, 586−596.

(8) Goyanes, A.; Det-Amornrat, U.; Wang, J.; Basit, A. W.; Gaisford, S. 3D Scanning and 3D Printing as Innovative Technologies for Fabricating Personalized Topical Drug Delivery Systems. *J. Controlled Release* **2016**, *234*, 41−48.

DOI: 10.1021/acsomega.8b03057
ACS Omega 2019, 4, 5412−5423

(9) Kalita, S. J.; Bose, S.; Hosick, H. L.; Bandyopadhyay, A. Development of Controlled Porosity Polymer-Ceramic Composite Scaffolds via Fused Deposition Modeling. *Mater. Sci. Eng., C* **2003**, *23*, 611−620.
(10) Goyanes, A.; Fernández-Ferreiro, A.; Majeed, A.; Gomez-Lado, N.; Awad, A.; Luaces-Rodríguez, A.; Gaisford, S.; Aguiar, P.; Basit, A. W. PET/CT Imaging of 3D Printed Devices in the Gastrointestinal Tract of Rodents. *Int. J. Pharm.* **2018**, *536*, 158−164.
(11) Nasereddin, J. M.; Wellner, N.; Alhijjaj, M.; Belton, P.; Qi, S. Development of a Simple Mechanical Screening Method for Predicting the Feedability of a Pharmaceutical FDM 3D Printing Filament. *Pharm. Res.* **2018**, *35*, 151.
(12) Zhang, J.; Feng, X.; Patil, H.; Tiwari, R. V.; Repka, M. A. Coupling 3D Printing with Hot-Melt Extrusion to Produce Controlled-Release Tablets. *Int. J. Pharm.* **2017**, *519*, 186−197.
(13) Kollamaram, G.; Croker, D. M.; Walker, G. M.; Goyanes, A.; Basit, A. W.; Gaisford, S. Low Temperature Fused Deposition Modeling (FDM) 3D Printing of Thermolabile Drugs. *Int. J. Pharm.* **2018**, *545*, 144−152.
(14) Kempin, W.; Franz, C.; Koster, L. C.; Schneider, F.; Bogdahn, M.; Weitschies, W.; Seidlitz, A. Assessment of Different Polymers and Drug Loads for Fused Deposition Modeling of Drug Loaded Implants. *Eur. J. Pharm. Biopharm.* **2017**, *115*, 84.
(15) Lim, S. H.; Kathuria, H.; Tan, J. J. Y.; Kang, L. 3D Printed Drug Delivery and Testing Systems — a Passing Fad or the Future? *Adv. Drug Delivery Rev.* **2018**, *132*, 139−168.
(16) Sadia, M.; Sośnicka, A.; Arafat, B.; Isreb, A.; Ahmed, W.; Kelarakis, A.; Alhnan, M. A. Adaptation of Pharmaceutical Excipients to FDM 3D Printing for the Fabrication of Patient-Tailored Immediate Release Tablets. *Int. J. Pharm.* **2016**, *513*, 659−668.
(17) Novák, M.; Boleslavská, T.; Grof, Z.; Waněk, A.; Zadražil, A.; Beránek, J.; Kovačík, P.; Štěpánek, F. Virtual Prototyping and Parametric Design of 3D-Printed Tablets Based on the Solution of Inverse Problem. *AAPS PharmSciTech* **2018**, 3414.
(18) Maroni, A.; Melocchi, A.; Parietti, F.; Foppoli, A.; Zema, L.; Gazzaniga, A. 3D Printed Multi-Compartment Capsular Devices for Two-Pulse Oral Drug Delivery. *J. Controlled Release* **2017**, *268*, 10−18.
(19) Beck, R. C. R.; Chaves, P. S.; Goyanes, A.; Vukosavljevic, B.; Buanz, A.; Windbergs, M.; Basit, A. W.; Gaisford, S. 3D Printed Tablets Loaded with Polymeric Nanocapsules: An Innovative Approach to Produce Customized Drug Delivery Systems. *Int. J. Pharm.* **2017**, *528*, 268−279.
(20) Okwuosa, T. C.; Soares, C.; Gollwitzer, V.; Habashy, R.; Timmins, P.; Alhnan, M. A. On Demand Manufacturing of Patient-Specific Liquid Capsules via Co-Ordinated 3D Printing and Liquid Dispensing. *Eur. J. Pharm. Sci.* **2018**, *118*, 134−143.
(21) Korte, C.; Quodbach, J. 3D-Printed Network Structures as Controlled-Release Drug Delivery Systems: Dose Adjustment, API Release Analysis and Prediction. *AAPS PharmSciTech* **2018**, 3333.
(22) Melocchi, A.; Parietti, F.; Loreti, G.; Maroni, A.; Gazzaniga, A.; Zema, L. 3D Printing by Fused Deposition Modeling (FDM) of a Swellable/Erodible Capsular Device for Oral Pulsatile Release of Drugs. *J. Drug Delivery Sci. Technol.* **2015**, *30*, 360−367.
(23) Goyanes, A.; Chang, H.; Sedough, D.; Hatton, G. B.; Wang, J.; Buanz, A.; Gaisford, S.; Basit, A. W. Fabrication of Controlled-Release Budesonide Tablets via Desktop (FDM) 3D Printing. *Int. J. Pharm.* **2015**, *496*, 414−420.
(24) Aho, J.; Boetker, J. P.; Baldursdottir, S.; Rantanen, J. Rheology as a Tool for Evaluation of Melt Processability of Innovative Dosage Forms. *Int. J. Pharm.* **2015**, *494*, 623−642.
(25) Zema, L.; Loreti, G.; Melocchi, A.; Maroni, A.; Gazzaniga, A. Injection Molding and Its Application to Drug Delivery. *J. Controlled Release* **2012**, *159*, 324−331.
(26) Combescot, E.; Morat, G.; de Lonlay, P.; Boudy, V. Pediatric Drug Formulation of Sodium Benzoate Extended-Release Granules. *Pharm. Dev. Technol.* **2016**, *21*, 261−267.
(27) Albertini, B.; Melegari, C.; Bertoni, S.; Dolci, L. S.; Passerini, N. A Novel Approach for Dry Powder Coating of Pellets with Ethylcellulose. Part II: Evaluation of Caffeine Release. *AAPS PharmSciTech* **2018**, *19*, 1426−1436.
(28) Elbadawi, M. Polymeric Additive Manufacturing: The Necessity and Utility of Rheology. In *Polymer Rheology*; Rivera-Armenta, J. L., Cruz, B. A. S., Eds.; IntechOpen: Rijeka, 2018; pp 43−63.
(29) Douglas, P.; Andrews, G.; Jones, D.; Walker, G. Analysis of in Vitro Drug Dissolution from PCL Melt Extrusion. *Chem. Eng. J.* **2010**, *164*, 359−370.
(30) Hashemi Sanatgar, R.; Campagne, C.; Nierstrasz, V. Investigation of the Adhesion Properties of Direct 3D Printing of Polymers and Nanocomposites on Textiles: Effect of FDM Printing Process Parameters. *Appl. Surf. Sci.* **2017**, *403*, 551−563.
(31) Gurney, R. S.; Dupin, D.; Nunes, J. S.; Ouzineb, K.; Siband, E.; Asua, J. M.; Armes, S. P.; Keddie, J. L. Switching Off the Tackiness of a Nanocomposite Adhesive in 30 s via Infrared Sintering. *ACS Appl. Mater. Interfaces* **2012**, *4*, 5442−5452.
(32) Hamed, G. R. Energy Conservation during Peel Testing. In *Treatise on Adhesion and Adhesives*; Patrick, R. L., Ed.; CRC Press, 1988; Vol. *6*, p 49.
(33) Chokshi, R. J.; Sandhu, H. K.; Iyer, R. M.; Shah, N. H.; Malick, A. W.; Zia, H. Characterization of Physico-Mechanical Properties of Indomethacin and Polymers to Assess Their Suitability for Hot-Melt Extrusion Process as a Means to Manufacture Solid Dispersion/Solution. *J. Pharm. Sci.* **2005**, *94*, 2463−2474.
(34) Sathigari, S. K.; Radhakrishnan, V. K.; Davis, V. A.; Parsons, D. L.; Babu, R. J. Amorphous-State Characterization of Efavirenz—polymer Hot-Melt Extrusion Systems for Dissolution Enhancement. *J. Pharm. Sci.* **2012**, *101*, 3456−3464.
(35) Wang, K.; Liang, S.; Zhao, P.; Qu, C.; Tan, H.; Du, R.; Zhang, Q.; Fu, Q. Correlation of Rheology−orientation−tensile Property in Isotactic Polypropylene/Organoclay Nanocomposites. *Acta Mater.* **2007**, *55*, 3143−3154.
(36) Solanki, N. G.; Tahsin, M.; Shah, A. V.; Serajuddin, A. T. M. Formulation of 3D Printed Tablet for Rapid Drug Release by Fused Deposition Modeling: Screening Polymers for Drug Release, Drug-Polymer Miscibility and Printability. *J. Pharm. Sci.* **2017**, 390.
(37) Boetker, J.; Water, J. J.; Aho, J.; Arnfast, L.; Bohr, A.; Rantanen, J. Modifying Release Characteristics from 3D Printed Drug-Eluting Products. *Eur. J. Pharm. Sci.* **2016**, *90*, 47.
(38) Holländer, J.; Genina, N.; Jukarainen, H.; Khajeheian, M.; Rosling, A.; Mäkilä, E.; Sandler, N. Three-Dimensional Printed PCL-Based Implantable Prototypes of Medical Devices for Controlled Drug Delivery. *J. Pharm. Sci.* **2016**, *105*, 2665−2676.
(39) Benwood, C.; Anstey, A.; Andrzejewski, J.; Misra, M.; Mohanty, A. K. Improving the Impact Strength and Heat Resistance of 3D Printed Models: Structure, Property, and Processing Correlationships during Fused Deposition Modeling (FDM) of Poly(Lactic Acid). *ACS Omega* **2018**, *3*, 4400−4411.
(40) Zhao, H.; Yan, X.; Zhao, G.; Guo, Z. Microcellular Injection Molded Polylactic Acid/Poly(ε-Caprolactone) Blends with Supercritical CO_2: Correlation between Rheological Properties and Their Foaming Behavior. *Polym. Eng. Sci.* **2016**, *56*, 939−946.
(41) Yan, Z.; Ye, L.; Zhang, A.; Feng, Z. The Mobility of Threaded α-Cyclodextrins in PR Copolymer and Its Influences on Mechanical Properties. *Chin. J. Polym. Sci.* **2017**, *35*, 752−763.
(42) Li, Z.; Liu, J.; Zhang, Z.; Gao, Y.; Liu, L.; Zhang, L.; Yuan, B. Molecular Dynamics Simulation of the Viscoelasticity of Polymer Nanocomposites under Oscillatory Shear: Effect of Interfacial Chemical Coupling. *RSC Adv.* **2018**, *8*, 8141−8151.
(43) Hornsby, P. R.; Mthupha, A. Rheological Characterization of Polypropylene Filled with Magnesium Hydroxide. *J. Mater. Sci.* **1994**, *29*, 5293−5301.
(44) Wu, G.; Zheng, Q. Estimation of the Agglomeration Structure for Conductive Particles and Fiber-Filled High-Density Polyethylene through Dynamic Rheological Measurements. *J. Polym. Sci., Part B: Polym. Phys.* **2004**, *42*, 1199−1205.

DOI: 10.1021/acsomega.8b03057
ACS Omega 2019, 4, 5412−5423

(45) Li, Y.; Zhu, J.; Wei, S.; Ryu, J.; Wang, Q.; Sun, L.; Guo, Z. Poly(Propylene) Nanocomposites Containing Various Carbon Nanostructures. *Macromol. Chem. Phys.* **2011**, *212*, 2429−2438.
(46) Lin, S.; Li, B.; Chen, T.; Yu, W.; Wang, X. Mechanical Reinforcement in Poly(Propylene Carbonate) Nanocomposites Using Double Percolation Networks by Dual Volume Exclusions. *Compos. Sci. Technol.* **2018**, *167*, 364−370.
(47) Marcin, W.; Benedito, A.; Gimenez, E. Preparation and Characterization of Extruded Nanocomposite Based on Polycarbonate/Butadiene-Acrylonitrile-Styrene Blend Filled with Multiwalled Carbon Nanotubes. *J. Appl. Polym. Sci.* **2014**, *131*, No. 40271.
(48) Song, N.; Zhu, L.; Yan, X.; Xu, Y.; Xu, X. Effect of Blend Composition on the Rheology Property of Polypropylene/Poly-(Ethylene-1-Octene) Blends. *J. Mater. Sci.* **2008**, *43*, 3218−3222.
(49) Li, H.; Huneault, M. A. Effect of Nucleation and Plasticization on the Crystallization of Poly(Lactic Acid). *Polymer* **2007**, *48*, 6855−6866.
(50) Martin, O.; Avérous, L. Poly(Lactic Acid): Plasticization and Properties of Biodegradable Multiphase Systems. *Polymer* **2001**, *42*, 6209−6219.
(51) Oh, H. J.; Freeman, B. D.; McGrath, J. E.; Ellison, C. J.; Mecham, S.; Lee, K.-S.; Paul, D. R. Rheological Studies of Disulfonated Poly(Arylene Ether Sulfone) Plasticized with Poly-(Ethylene Glycol) for Membrane Formation. *Polymer* **2014**, *55*, 1574−1582.
(52) Vieira, M. G. A.; da Silva, M. A.; dos Santos, L. O.; Beppu, M. M. Natural-Based Plasticizers and Biopolymer Films: A Review. *Eur. Polym. J.* **2011**, *47*, 254−263.
(53) Salehiyan, R.; Hyun, K. Effect of Organoclay on Non-Linear Rheological Properties of Poly(Lactic Acid)/Poly(Caprolactone) Blends. *Korean J. Chem. Eng.* **2013**, *30*, 1013−1022.
(54) Takhulee, A.; Takahashi, Y.; Vao-soongnern, V. Molecular Simulation and Experimental Studies of the Miscibility of Polylactic Acid/Polyethylene glycol Blends. *J. Polym. Res.* **2017**, *24*, 8.
(55) Lin, W. J.; Lee, H. K.; Wang, D. M. The Influence of Plasticizers on the Release of Theophylline from Microporous-Controlled Tablets. *J. Controlled Release* **2004**, *99*, 415−421.
(56) Luo, C.; Chen, W.; Gao, Y. Fractional Crystallization Behavior of PCL and PEG in Blends. *Polym. Sci., Ser. A* **2016**, *58*, 196−205.
(57) Lin, W.-J.; Lu, C.-H. Characterization and Permeation of Microporous Poly(ε-Caprolactone) Films. *J. Membr. Sci.* **2002**, *198*, 109−118.
(58) Liu, L.; Wang, Y.; Guo, S.; Wang, Z.; Wang, W. Porous Polycaprolactone/Nanohydroxyapatite Tissue Engineering Scaffolds Fabricated by Combining NaCl and PEG as Co-Porogens: Structure, Property, and Chondrocyte−scaffold Interaction in Vitro. *J. Biomed. Mater. Res., Part B* **2012**, *100B*, 956−966.
(59) Nuchitprasitchai, S.; Roggemann, M.; Pearce, J. M. Factors Effecting Real-Time Optical Monitoring of Fused Filament 3D Printing. *Prog. Addit. Manuf.* **2017**, *2*, 133−149.
(60) Armillotta, A.; Bellotti, M.; Cavallaro, M. Warpage of FDM Parts: Experimental Tests and Analytic Model. *Rob. Comput.-Integr. Manuf.* **2018**, *50*, 140−152.
(61) Chang, T. C.; Faison, E. Shrinkage Behavior and Optimization of Injection Molded Parts Studied by the Taguchi Method. *Polym. Eng. Sci.* **2001**, *41*, 703−710.
(62) Averous, L.; Moro, L.; Dole, P.; Fringant, C. Properties of Thermoplastic Blends: Starch−polycaprolactone. *Polymer* **2000**, *41*, 4157−4167.
(63) Siegmann, A.; Buchman, A.; Kenig, S. Residual Stresses in Polymers. II. Their Effect on Mechanical Behavior. *Polym. Eng. Sci.* **1981**, *21*, 997−1002.
(64) Lin, S.-Y.; Lee, C.-J.; Lin, Y.-Y. The Effect of Plasticizers on Compatibility, Mechanical Properties, and Adhesion Strength of Drug-Free Eudragit E Films. *Pharm. Res.* **1991**, *8*, 1137−1143.
(65) Lin, S.-Y.; Chen, K.-S.; Run-Chu, L. Organic Esters of Plasticizers Affecting the Water Absorption, Adhesive Property, Glass Transition Temperature and Plasticizer Permanence of Eudragit Acrylic Films. *J. Controlled Release* **2000**, *68*, 343−350.
(66) Cilurzo, F.; Gennari, C. G. M.; Minghetti, P. Adhesive Properties: A Critical Issue in Transdermal Patch Development. *Expert Opin. Drug Delivery* **2012**, *9*, 33−45.
(67) Gullick, D. R.; Pugh, W. J.; Ingram, M. J.; Cox, P. A.; Moss, G. P. Formulation and Characterization of a Captopril Ethyl Ester Drug-in-Adhesive-Type Patch for Percutaneous Absorption. *Drug Dev. Ind. Pharm.* **2010**, *36*, 926−932.
(68) Michaelis, M.; Brummer, R.; Leopold, C. S. Plasticization and Antiplasticization of an Acrylic Pressure Sensitive Adhesive by Ibuprofen and Their Effect on the Adhesion Properties. *Eur. J. Pharm. Biopharm.* **2014**, *86*, 234−243.
(69) Repka, M. A.; McGinity, J. W. Physical−mechanical, Moisture Absorption and Bioadhesive Properties of Hydroxypropylcellulose Hot-Melt Extruded Films. *Biomaterials* **2000**, *21*, 1509−1517.
(70) Fisher, D. G.; Rowe, R. C. The Adhesion of Film Coatings to Tablet Surfaces—Instrumentation and Preliminary Evaluation. *J. Pharm. Pharmacol.* **1976**, *28*, 886−889.
(71) Rowe, R. C. Microindentation - a Method for Measuring the Elastic Properties and Hardness of Films on Conventionally Coated Tablets. *J. Pharm. Pharmacol.* **1976**, *28*, 310−311.
(72) Gullapalli, R. P.; Mazzitelli, C. L. Polyethylene Glycols in Oral and Parenteral Formulations—A Critical Review. *Int. J. Pharm.* **2015**, *496*, 219−239.
(73) Li, F.-J.; Zhang, S.-D.; Liang, J.-Z.; Wang, J.-Z. Effect of Polyethylene Glycol on the Crystallization and Impact Properties of Polylactide-Based Blends. *Polym. Adv. Technol.* **2015**, *26*, 465−475.
(74) Sreedhar, B.; Chattopadhyay, D. K.; Karunakar, M. S. H.; Sastry, A. R. K. Thermal and Surface Characterization of Plasticized Starch Polyvinyl Alcohol Blends Crosslinked with Epichlorohydrin. *J. Appl. Polym. Sci.* **2006**, *101*, 25−34.

DOI: 10.1021/acsomega.8b03057
ACS Omega 2019, 4, 5412−5423